

Shape coexistence scenario in ^{150}Sm from a γ - γ fast-timing measurement

S. Basak,^{1,2} S. S. Alam^{1,2,*}, D. Kumar,^{1,2} A. Saha,^{1,†} and T. Bhattacharjee^{1,2,‡}

¹Variable Energy Cyclotron Centre, Kolkata - 700 064, India

²Homi Bhabha National Institute, Training School Complex, Anushakti Nagar, Mumbai - 400 094, India

 (Received 4 December 2020; revised 9 July 2021; accepted 30 July 2021; published 12 August 2021)

Lifetimes are measured for low lying states of ^{150}Sm , populated from β^- decay of ^{150}Pm produced through (p, n) reactions with a ^{150}Nd target. The VENTURE array comprising of eight fast CeBr₃ detectors is used for lifetime measurement with γ - γ fast timing technique. The lifetime of 0_3^+ level of ^{150}Sm is measured for the first time to be 36(10) ps. The 0_3^+ level is found to have enhanced decay strengths to the $K^\pi = 0_2^+$ structure compared with $K^\pi = 0_1^+$. A high $\rho^2(E0)$ strength for the $0_3^+ \rightarrow 0_2^+$ decay confirms shape coexistence and shape mixing in $N = 88$ ^{150}Sm .

DOI: 10.1103/PhysRevC.104.024320

I. INTRODUCTION

The presence of multiple close lying eigenstates with different intrinsic deformation in a finite nuclear many-body quantum system is known as shape coexistence [1]. It is closely related to the shell gaps and the nature of particle-hole excitations leading to an induced deformation around the spherical (deformed) structures of the ground state. The nuclei around $Z = 64$ and $N = 90$, especially the Sm and Gd isotopes, provide the classical examples of shape coexistence and shape phase transitions with interesting observations already made through decades [2–6]. However, understanding shape coexistence is still challenging and there exist unsolved problems that require more attention on the low-lying excited levels as a function of N and Z . One of these to mention is the underlying structure of the excited 0^+ levels in even-even nuclei that are not understood completely and are of contemporary interest [7–11].

The two-nucleon transfer data from (p, t) reactions [12] suggests the shape coexisting features of the 0^+ levels in ^{150}Sm and ^{152}Sm . In this work, the 0_3^+ levels of ^{150}Sm and ^{152}Sm are observed to have different deformation in coexistence with their near spherical and deformed ground states, respectively. In case of ^{152}Sm , which is described as the critical point of the first-order phase transition from spherical vibrator to axial rotor [13], the 0_3^+ level was described as a pairing isomer [14]. On the contrary, such description for ^{152}Sm was contradicted by Mach *et al.* [15] and by Gupta and Hamilton [16]. In the work by Mach *et al.* [15], all the 0^+ bands in ^{152}Sm are interpreted to follow quadrupole phonon multiplet structures [17] from energy, $B(E2)$ and the $\rho^2(E0)$

systematics. In the work of Gupta and Hamilton [16], all low-lying 0^+ levels have been interpreted to have similar rotational character, so rejecting the shape coexistence and/or pairing isomer pictures for these levels.

Similarly, in case of ^{150}Sm also, the 0_3^+ state was found to correspond to a deformed structure [18] in coexistence with its near spherical ground state. Whereas the recent work by Gupta, Kumar, and Hamilton [19] proposes the 0_3^+ (1255 keV), 2_4^+ (1417 keV), and 4_4^+ (1819 keV) levels to be the candidates of a $K = 0$ band having a quasirotational $\beta\beta$ two phonon structure. Their interpretation is based on the $E(0_3^+)/E(0_2^+)$ ratio of 1.7, presence of γ transition from $0_3^+ \rightarrow 2_2^+$ (level of $K = 0$, β vibrational band) and from the $B(E2)$ values obtained from dynamic pairing plus quadrupole (DPPQ) model calculations. Such structure was further supported by the observation of another γ transition from the 2_4^+ level to the 2_2^+ level of $K = 0$, β vibrational band [20].

The transition strengths, $B(E2)$ and the $\rho^2(E0)$, from the low-lying excited levels in the even-even nuclei are shown to be the best direct indicators in identifying the shapes, deformation, and their coexistence [1, 2, 4, 21, 22]. So, measuring the $E0$ and $E2$ transition strengths in ^{150}Sm ($N = 88$) is important in the context of shape coexistence around $N = 90$. However, the population of the 0_3^+ level in this nucleus has been observed only in decay, neutron-induced reactions and transfer reactions, but not in any fusion evaporation reaction giving rise to high yield. In the present work, lifetime measurements have been carried out for the low-lying levels in ^{150}Sm , viz., 2_1^+ (334 keV), 0_2^+ (740 keV), and 0_3^+ (1255 keV), using γ - γ fast timing spectroscopy with VECC array for nuclear fast timing and angular Correlation studies (VENTURE array) [23] and populating the excited levels from beta decay of ^{150}Pm .

II. EXPERIMENT

The low-lying excited states of ^{150}Sm were populated from the β^- decay of ^{150}Pm . The $^{150}\text{Nd}(p, n)^{150}\text{Pm}$ reaction was used with 8.0 MeV proton beam, provided by

*Present address: Government General Degree College, Chapra, West Bengal, India.

†Present address: Department of Physics, ICFAI University, Tripura, India.

‡btumpa@vecc.gov.in

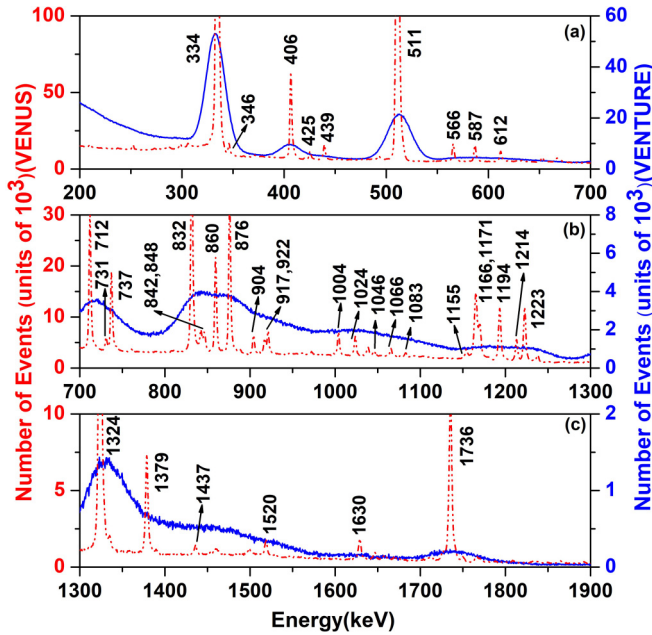


FIG. 1. The CeBr₃ (blue, solid) and Clover (red, dash-dot-dot) total projections obtained from CeBr₃-CeBr₃ and CeBr₃-Clover coincidence data, respectively. This was used to identify the deexciting γ lines from excited level of ¹⁵⁰Sm, as detected in CeBr₃ and Clover detectors of the setup.

$K = 130$ AVF cyclotron at the Variable Energy Cyclotron Centre (VECC), Kolkata, India, to produce the parent ¹⁵⁰Pm. The maximum production of ¹⁵⁰Pm and minimization of contaminations were ensured by using the appropriate beam energy and the use of a commercially available 97.65% enriched target. More details on the population of ¹⁵⁰Pm can be found in Ref. [20]. The targets were irradiated with stacked foil irradiation technique and were subsequently counted with the VENTURE array [23] consisting of eight 1" \times 1" fast CeBr₃ detectors, coupled with six Compton-suppressed Clover HPGe detectors of the VENUS array [20]. Repeated irradiations and countings were performed with appropriate cooling time for gaining γ - γ statistics. The CeBr₃ total projection from the CeBr₃-CeBr₃ coincidences is shown in Fig. 1 and is compared with the Clover total projection from CeBr₃-Clover coincidences. These total projections are obtained without any subtraction of the underlying background. The comparative spectra could identify the strong γ peaks in ¹⁵⁰Sm.

The time resolution for a combination of two CeBr₃ detectors of the VENTURE array is known to be 154(8) ps at the γ energy of ⁶⁰Co decay and is 188(3) ps for the array [23]. The generalized centroid difference (GCD) method [24] was used for lifetime measurement after detecting the deexciting γ radiations in coincidence mode. More details on the characteristics of the detectors, the VENTURE array, the electronics setup, and the γ - γ fast timing analysis technique used in the present work can be found in Ref. [23]. The prompt response difference (PRD) curve, representing the prompt time characteristics of the array, has been generated for the analysis of γ - γ fast timing data taken with a ¹⁵²Eu

source. The prompt response depends on the PMT voltages, CFD settings, detector geometry, etc., along with other long-term effects which have been constantly monitored during the experiment. In the present work, the PRD curve shown in Fig. 19 of Ref. [23] has been used, as the present measurement was carried out with the same detector and electronics setup reported in Ref. [23], also used for detailed description of the VENTURE characteristics.

III. RESULTS

During the lifetime measurement using GCD method, the delayed and antidelayed time difference distributions for different γ - γ cascades are studied to find out the experimental centroid difference (ΔC_{expt}). In the present work, energy gates about 15–20 keV has been used for the analysis of different cascades except for the weak ones where the range has been increased to obtain sufficient statistics in the delayed and antidelayed projections. Appropriate background corrections were employed following methods described in Refs. [25,26] to determine the background related centroid differences (ΔC_{BG} for feeder and decay). The peak to background ratios (p/b) required to determine the background corrections [t_{corr} (feeder), t_{corr} (decay), and t_{corr}] were estimated from the energy gated projections. The centroid differences corresponding to the full energy peak (FEP) (ΔC_{FEP}) were subsequently obtained after correcting the ΔC_{expt} with t_{corr} . The prompt time reference, determined from the calibrated prompt time curve of the VENTURE array was used for measuring the level lifetimes from the ΔC_{FEP} values. Three standard deviation ($3\sigma \approx 9$ ps) obtained in the prompt time calibration was considered while calculating the error in the measured lifetime ($\delta\tau$). Details of analysis procedure, using the following sets of equations, can be found in Refs. [23,25,26].

$$\Delta C_{\text{FEP}} = \Delta C_{\text{expt}} + t_{\text{corr}}, \quad (1)$$

where

$$t_{\text{corr}} = \frac{p/b(E_{\text{decay}})t_{\text{corr}}(\text{feeder}) + p/b(E_{\text{feeder}})t_{\text{corr}}(\text{decay})}{p/b(E_{\text{feeder}}) + p/b(E_{\text{decay}})},$$

where

$$t_{\text{corr}}(\text{feeder}) = \left[\frac{\Delta C_{\text{expt}} - \Delta C_{\text{BG}}}{p/b} \right]_{\text{feeder}},$$

$$t_{\text{corr}}(\text{decay}) = \left[\frac{\Delta C_{\text{expt}} - \Delta C_{\text{BG}}}{p/b} \right]_{\text{decay}},$$

for $p/b(E_{\text{feeder}}) \sim p/b(E_{\text{decay}})$, t_{corr} simplifies to

$$t_{\text{corr}} = \frac{1}{2}[t_{\text{corr}}(\text{feeder}) + t_{\text{corr}}(\text{decay})],$$

$$\tau = \frac{1}{2}[\Delta C_{\text{FEP}} - \text{PRD}],$$

$$\delta\tau = \frac{1}{2}\sqrt{(\delta\Delta C_{\text{expt}})^2 + (\delta t_{\text{corr}})^2 + (\delta\text{PRD})^2}. \quad (2)$$

Figures 2 and 3 demonstrate the analysis procedure used for the lifetime measurement in the present work, considering the known case of (i) 1324–334 keV cascade for 2_1^+ level and

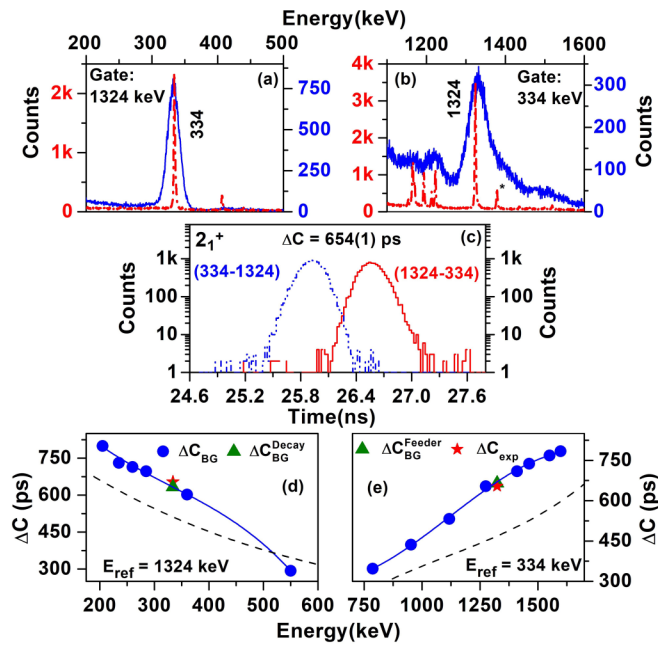


FIG. 2. The CeBr_3 energy-gated projections of CeBr_3 (blue, solid) and Clover (red, dash-dot) detectors are shown with gate on (a) feeder (1324 keV) and (b) decay (334 keV) γ rays of 1324–334 keV cascade corresponding to 2_1^+ level. The delayed (red, solid) and antidelayed (blue, dash-dot-dot) time difference spectra are shown in panel (c). The background analysis for this cascade are shown in panels (d) and (e) where ΔC_{BG} values are shown with respect to $\text{PRD} = 0$ at E_{ref} . The PRD curve is also shown with black dashed line by making $\text{PRD} = 0$ at E_{ref} . The $\Delta C = 0$ line is out of the scale of the background plot and is not shown.

(ii) 1223–406 keV cascade for 0_2^+ level. In these figures, the gated projections corresponding to CeBr_3 gates for (a) E_{feeder} and (b) E_{decay} , respectively, are shown from the CeBr_3 - CeBr_3 coincidences. To look for the neighboring γ rays which may falsify the results, the gated projections from CeBr_3 -Clover coincidences are also shown. However, the later set of data is involved with a long coincidence time gate and may include some random coincidences. The clean projections obtained for the 334–1324 keV cascade was used for the generation of delayed and antidelayed time projections. The appearance of 1379 keV (marked with *) near the 1324 keV could not be avoided as this transition has a true coincidence with 334 keV and corresponds to the 2_1^+ level only, for which lifetime is measured. In case of 1223–406 keV cascade, γ peaks are observed neighboring to 1223 keV peak in the CeBr_3 -Clover data that may arise from the coincidence with Compton or random background (shown with #). The range of gate used in the analysis of this cascade has been shown with solid vertical lines [Fig. 3(b)]. In such cases, in addition to the careful choice of energy gate, an error of 3 ps ($\approx 1\sigma$) has also been added to the measured lifetime value as done in Refs. [25,27]. The delayed and antidelayed time spectra (c), that have been generated for a particular cascade, are shown in the corresponding figures. In addition, the background analysis is also demonstrated, both around (d) E_{decay} and (e) E_{feeder} , respectively, in both Figs. 2 and 3. The background

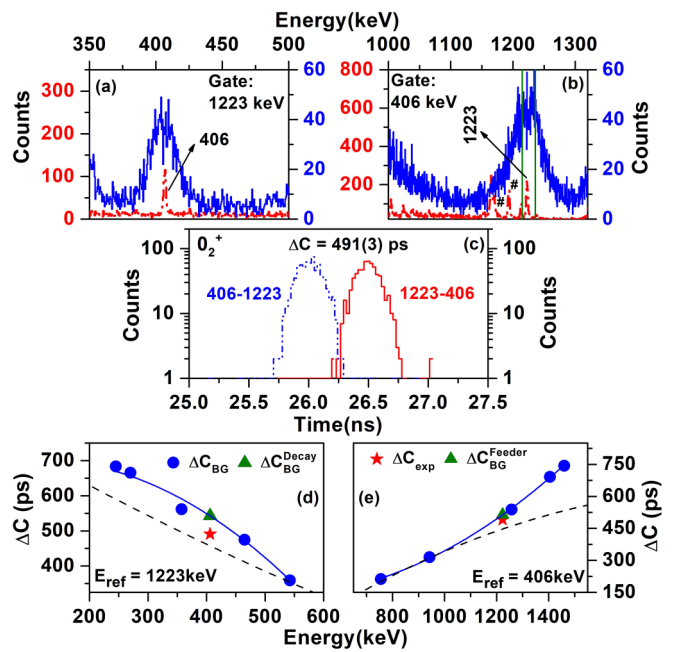


FIG. 3. The CeBr_3 energy gated projections of CeBr_3 (blue, solid) and Clover (red, dash-dot) detectors are shown with gate on (a) feeder (1223 keV) and (b) decay (406 keV) γ rays of 1223–406 keV cascade (0_2^+ level). The delayed (red, solid) and antidelayed (blue, dash-dot-dot) time difference spectra are shown in panel (c). The background analysis for this cascade are shown in panels (d) and (e) where ΔC_{BG} values are shown with respect to $\text{PRD} = 0$ at E_{ref} . The PRD curve is also shown with black dashed line by making $\text{PRD} = 0$ at E_{ref} . The $\Delta C = 0$ line is out of the scale of the background plot and is not shown. The peaks neighboring to the gamma line of interest are shown which are arising out of coincidence with underlying Compton background or random (#). The range of γ gates given in such cases for the generation of time distribution spectra are shown with solid vertical lines.

corrections are shown with respect to the PRD curve drawn with $\text{PRD} = 0$ at the reference energy value. For both of these cases (2_1^+ and 0_2^+), the known lifetimes [28] were reasonably reproduced in the present work.

Following the verification on the known cases, the lifetime was measured for the 0_3^+ level of ^{150}Sm . The analyzed data are shown for the 1004–922 keV cascade corresponding to 0_3^+ level in Fig. 4. The energy gates have been chosen carefully to avoid possible contaminations with a clean selection of the relevant cascade and the ranges are shown with solid vertical lines on Fig. 4. With such a selection, the 1024 keV transition, observed in 922 keV gate, was found to originate mainly from the Compton-photoppeak coincidence and could be corrected during background subtraction procedure employed in GCD analysis. In addition, an extra systematic error of 3 ps was also added to this result to consider the effect from 917–1046 keV coincidence associated with a 0.86 ps lifetime of 1046 keV level, if any. The delayed and antidelayed time projections as well as the background analyses for 0_3^+ level are also shown in Fig. 4.

The lifetimes measured in the present work are listed in Table I with all the ΔC and p/b values that were relevant

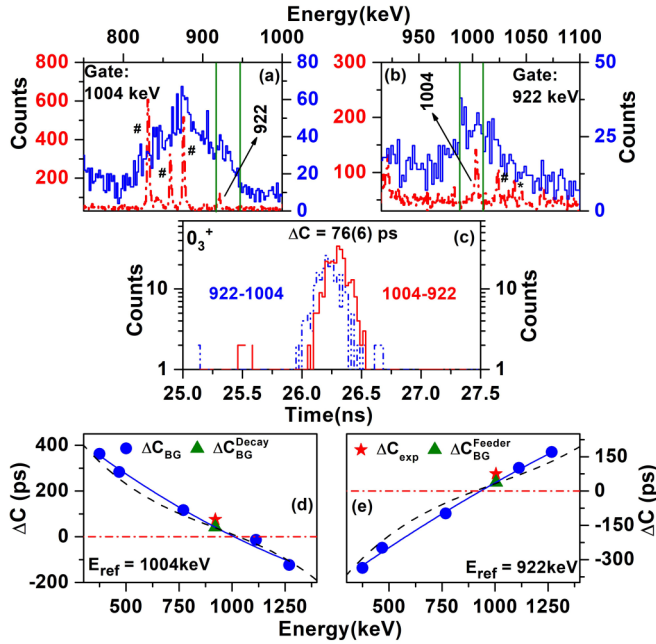


FIG. 4. The CeBr₃ energy gated projections of CeBr₃ (blue, solid) and Clover (red, dash-dot) detectors are shown with gate on (a) feeder (1004 keV) and (b) decay (922 keV) γ rays of 1004-922 keV cascade corresponding to the 0_3^+ level. The delayed (red, solid) and antidelayed (blue, dash-dot-dot) time difference spectra are shown in (c). The background analysis for this cascade are shown in panels (d) and (e) where ΔC_{BG} values are shown with respect to PRD = 0 at E_{ref} . The PRD curve is also shown with black dashed line by making PRD = 0 at E_{ref} . The red dash-dotted line is drawn to guide the eye for ΔC or PRD = 0. The peaks neighboring to the gamma line of interest in panels (a) and (b) are shown, which are arising out of coincidence with photopeak (*), underlying Compton background or random (#). The range of γ gates given in such cases for the generation of time distribution spectra to minimize the effect of contamination are shown with solid vertical lines.

to arrive at the final results. The measured lifetimes are also compared with earlier data, if available in literature. The present work finds the lifetimes of 2_1^+ and 0_2^+ levels in reasonable agreement with the evaluated data [28]. The lifetime has been measured for the first time for the 0_3^+ level in ^{150}Sm and it comes out to be 36(10) ps. The $B(E2)$ and $\rho^2(E0)$ values have been estimated from the measured lifetime using

equations

$$B(E2) = \frac{1}{1.22 \times 10^9 \times E_\gamma^5 \tau_p} e^2 \text{ fm}^4, \quad (3)$$

$$B(E2)_{1 \text{ w.u.}} = 0.0594 A^{\frac{4}{3}} e^2 \text{ fm}^4,$$

$$\rho^2(E0) = \frac{\chi(E0/E2)B(E2)}{e^2 R^4}, \quad (4)$$

where τ_p is the partial level lifetime that has been calculated from the measured level lifetime τ considering the branching and mixing ratios. The term χ is defined as $\chi(E0/E2) = \frac{B(E0)}{B(E2)}$ and has been taken from Ref. [29] for calculation of $E0$ transition strengths. During this calculation for both 0_2^+ and 0_3^+ levels in ^{150}Sm , corresponding $B(E2)$ strength for their decay to 2_1^+ level was considered, as available from Ref. [29]. The branching ratios were taken from Table V of Ref. [30], as this work reports new gamma transitions and so modified branching ratios. The $E0$ branching was taken from ENSDF [28] and the conversion coefficients were calculated using BrIcc code [31]. The progression of error in $B(E2)$ values were estimated following Ref. [32,33] and was found to be asymmetric for the cases that are associated with large error in lifetime results.

The estimated $E2$ and $E0$ transition strengths are tabulated in Table II along with the values from different theoretical model calculations, available in literature, like the interacting boson model (IBM) and the DPPQ model [19], respectively. It is found that the measured $B(E2)$ values are well reproduced by the theoretical calculations, wherever available. The $\rho^2(E0)$ values for the $0_2^+ \rightarrow 0_1^+$ decay were also calculated by considering the IBM and DPPQ results for $B(E2)$ ($0_2^+ \rightarrow 2_1^+$) and the $\chi(E0/E2)$ from Ref. [29] and are shown in Table II.

IV. DISCUSSION

The relevant levels for ^{150}Sm and their decay have been compared with the same in the neighboring ^{152}Sm in Fig. 5. In this figure, the width of the $E2$ transitions indicate the $B(E2)$ values and that of $E0$ transitions indicate the $\rho^2(E0) \times 10^3$ values. The $E0$ transitions are shown with red.

The comparison of relevant energy spacings among the levels of ground state band and the $B(E2)$ ($2_1^+ \rightarrow 0_1^+$) of these two nuclei clearly indicate that ^{152}Sm has more deformation compared with ^{150}Sm in their ground state. It is observed that the same trend follows for the $K^\pi = 0_\beta^+$ and $K^\pi = 2_\gamma^-$ band

TABLE I. Lifetime results for the low-lying levels of ^{150}Sm , for which measurements have been carried out in the present work, are shown in bold. The lifetimes are calculated by using the equation: $\tau = \frac{1}{2}(\Delta C_{FEP} - \text{PRD})$. The quoted errors in lifetime are calculated by considering the standard deviation, i.e., $3\sigma \approx 9$ ps, obtained in the generation of PRD curve and the errors estimated for the ΔC values.

E_x (keV)	J^π	Cascade (keV)	ΔC_{expt} (ps)	ΔC_{BG} (ps)	p/b	ΔC_{BG}		t_{corr} (ps)	ΔC_{FEP} (ps)	PRD (ps)	Lifetime (τ) (ps)	
						(feeder)	(decay)				Pres. work	Lit. [28]
334	2_1^+	1324–334	654(1)	665(6)	2.82(5)	633(8)	15.2(4)	−3(2)	651(2)	494	79(8)	69.8(16)
		1736–334	853(6)	868(7)	1.29(7)	939(28)	14.6(8)	−12(7)	841(9)	677	82(9)	
740	0_2^+	1223–406	491(3)	514(1)	1.67(9)	543(12)	2.13(12)	−18(3)	473(4)	403	35(8)	28.4(27)
1255	0_3^+	1004–922	76(6)	38(6)	1.04(9)	42(11)	1.02(9)	35(8)	111(10)	39	36(10)	

TABLE II. $B(E2)$ and $\rho^2(E0)$ values for the low-lying levels of ^{150}Sm measured in the present work. The $B(E2)$ values calculated using IBM and DPPQ models are taken from Ref. [19] and shown wherever available.

J_i	$\rightarrow J_f$	E_γ (keV)	Multipolarity	Experiment		Theory	
				$B(E2)$ (W.u.)	$\rho^2(E0)$ (10^{-3})	DPPQ	IBM
				Pres. work		Ref. [19]	
2_1^+	$\rightarrow 0_1^+$	334	$E2$	$50_{(-5)}^{(+6)}$		72	46
0_2^+	$\rightarrow 2_1^+$	406	$E2$	$44_{(-8)}^{(+13)}$		84	63
	$\rightarrow 0_1^+$	740	$E0$		$15_{(-3)}^{(+5)}$	29 ^a	22 ^a
0_3^+	$\rightarrow 2_2^+$	209	$E2$	$92_{(-20)}^{(+36)}$		106	
	$\rightarrow 0_2^+$	515	$E0$		$101_{(-22)}^{(+39)}$		
	$\rightarrow 2_1^+$	922	$E2$	$0.56_{(-12)}^{(+21)}$			
	$\rightarrow 0_1^+$	1256	$E0$		$4_{(-1)}^{(+1)}$		

^aThe $\rho^2(E0)$ values corresponding to decay of 0_2^+ level are calculated using $B(E2)$ values from Ref. [19] and χ values from Ref. [29].

but not for the $K^\pi = 0_3^+$ band which has higher energy spacing in case of $N = 90$ Sm. It is observed that the deduced $B(E2)$ strengths also follow the same systematics as observed from the energy spacings.

The $B(E2)$ and $\rho^2(E0)$ values for the decays associated with different excited 0^+ levels help in identifying the structure of these levels and high $E0$ strengths indicate the coexistence and mixing of shapes in a nucleus [2,4]. The comparative $B(E2)$ and $\rho^2(E0)$ strengths for the decays of 0_2^+ and 0_3^+ levels in ^{150}Sm , obtained in the present work, are shown in Fig. 6 in comparison to the neighboring Sm and Gd nuclei around $N = 90$. The $B(E2)$ value for the $0_3^+ \rightarrow 2_2^+$ decay in $N = 88$ Sm indicates strong collectivity and is found to be following the systematics in the neighboring nuclei. This could not, however, be compared with the systematics of 0_3^+ decays with varying Z in this region as the absolute transition strengths are not experimentally measured for any other case.

In both $N = 88, 90$ Sm nuclei, the deduced absolute $E2$ strengths for the decay of the 0_3^+ level to the ground-state band do not satisfy the criteria for this level to be interpreted as a candidate of beta vibration [10]. On the contrary, it is observed that the 0_3^+ state has stronger decay strengths to the $K^\pi = 0_2^+$ band compared with that to the ground band. In the present work, the ratio of $B(E2)$ ($0_3^+ \rightarrow 2_2^+/B(E2)$ ($0_3^+ \rightarrow 2_1^+$) in ^{150}Sm comes out to be $164_{(-50)}^{(+89)}$ ($\approx 0.16_{(-5)}^{(+9)} \times 10^3$). The said $B(E2)$ ratio was found to be 2.5×10^3 from DPPQ and 10^4

from IBM model calculations, respectively [19]. In the case of ^{152}Sm , the $B(E2)$ ($0_3^+ \rightarrow 2_2^+/B(E2)$ ($0_3^+ \rightarrow 2_1^+$) ratio is found to be 40(23) which is reported as >40 [28] and was predicted as 126 and 368 by DPPQ and IBM calculations [16], respectively.

The $\rho^2(E0)$ strengths for the $0_2^+ \rightarrow 0_1^+$ decay show similar trends in both Sm and Gd nuclei, giving a higher value at $N = 90$. However, the said strength for $0_3^+ \rightarrow 0_2^+$ decay in Sm reduces from $N = 88$ to $N = 90$. As there is no other data available in literature for the lifetime of 0_3^+ levels around $N = 90$, the systematics could not be verified for a wider range of proton and neutron numbers.

The $E0$ strength for the decay of 0_3^+ level to the 0_2^+ level comes out to be $101_{(-22)}^{(+39)} \times 10^{-3}$ unit which is very high and is similar to that calculated for $N = 90$ ^{154}Gd [29]. The $E0$ strength of $39(3) \times 10^{-3}$ unit measured for 0_2^+ level in ^{152}Gd

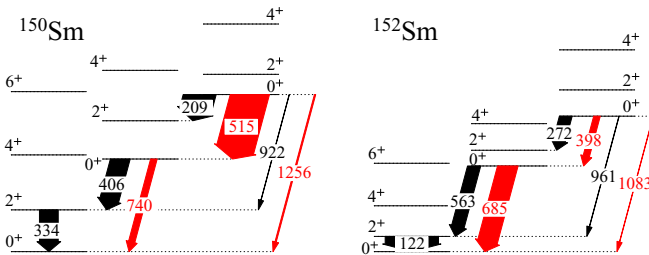


FIG. 5. The partial level schemes of ^{150}Sm and ^{152}Sm are compared for the decays from the excited 0_2^+ and 0_3^+ levels. The width of the transitions indicate the corresponding reduced transition strengths. The $E0$ decays are shown in red and the $E2$ decays in black. See text for details.

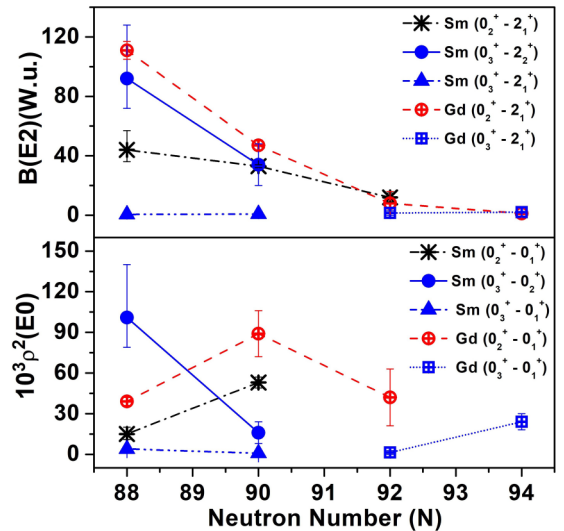


FIG. 6. The $B(E2)$ and $\rho^2(E0)$ values for the decays of 0_2^+ and 0_3^+ levels in Sm and Gd nuclei are shown as a function of neutron number. The $B(E2)$ value for $N = 88$ Sm has been taken from present work and that of 0_2^+ levels of Gd isotopes are taken from Ref. [22]. The other values shown are deduced from the known lifetimes in literature [34]. The $\rho^2(E0)$ values have been calculated from the $B(E2)$ values.

was established as the signature of quantum shape phase transition in this nucleus [22]. The relationship of shape coexistence and shape mixing with high $\rho^2(E0)$ is also described in Refs. [2,4]. Therefore, the high $E0$ strength obtained in the present work confirms the occurrence of first-order quantum shape phase transition and shape mixing in $N = 88$ Sm.

V. SUMMARY

The lifetimes have been measured for three low-lying levels in ^{150}Sm , populated from the β decay of ^{150}Pm . The present work provides the first experimental lifetime data for the 0_3^+ level in $N = 88$ Sm nucleus. The transition strengths $B(E2)$ and $\rho^2(E0)$ have been deduced from experimentally measured lifetimes and are compared with the theoretical calculations as well as with those available in the neighboring nuclei. The high $\rho^2(E0)$ value obtained for the 0_3^+ level in

$N = 88$ Sm suggests the quantum shape phase transition as expected around $N = 90$. It is observed that the 0_3^+ levels have stronger absolute transition strengths to the $K^\pi = 0_2^+$ configuration in $N = 88$ and 90 Sm nuclei.

ACKNOWLEDGMENTS

The authors gratefully acknowledge the valuable suggestions from Prof. W. Urban, University of Warsaw, Poland. The effort of cyclotron staffs at VECC for providing good quality beam is sincerely acknowledged. Dr. D. Banerjee of RCD, VECC is acknowledged for his help in irradiation and target preparation. I. Saikh and A. Chowdhury of the Physics Lab, VECC are acknowledged for maintaining the setup during the experiment. S. Basak acknowledges the fellowship from University Grants Commission, India.

-
- [1] K. Heyde and J. L. Wood, *Rev. Mod. Phys.* **83**, 1467 (2011).
 [2] P. Cejnar, J. Jolie, R. F. Casten, *Rev. Mod. Phys.* **82**, 2155 (2010).
 [3] J. H. Bjerregaard, O. Hansen, O. Nathan, and S. Hinds, *Nucl. Phys.* **86**, 145 (1966).
 [4] J. L. Wood, E. F. Zganjar, C. De Coster, and K. Heyde, *Nucl. Phys. A* **651**, 323 (1999).
 [5] W. D. Kulp *et al.*, *Phys. Rev. C* **77**, 061301(R) (2008).
 [6] P. E. Garrett *et al.*, *Phys. Rev. Lett.* **103**, 062501 (2009).
 [7] A. Gottardo *et al.*, *Phys. Rev. Lett.* **116**, 182501 (2016).
 [8] A. Aprahamian, R. C. de Haan, S. R. Leshner, C. Casarella, A. Stratman, H. G. Börner, H. Lehmann, M. Jentschel, and A. M. Bruce, *Phys. Rev. C* **98**, 034303 (2018).
 [9] W. D. Kulp, J. L. Wood, K. S. Krane, J. Loats, P. Schmelzenbach, C. J. Staples, R.-M. Larimer, and E. B. Norman, *Phys. Rev. Lett.* **91**, 102501 (2003).
 [10] P. E. Garrett, *J. Phys. G* **27**, R1 (2001).
 [11] J. F. Sharpey-Schafer, R. A. Bark, S. P. Bvumbi, T. R. S. Dinoko, and S. N. T. Majola, *Eur. Phys. J. A* **55**, 15 (2019).
 [12] W. McLatchie, W. Darcey, and J. E. Kitching, *Nucl. Phys. A* **159**, 615 (1970).
 [13] R. F. Casten and N. V. Zamfir, *Phys. Rev. Lett.* **87**, 052503 (2001).
 [14] W. D. Kulp *et al.*, *Phys. Rev. C* **71**, 041303(R) (2005).
 [15] H. Mach, M. Hellström, B. Fogelberg, D. Jerrestam, and L. Spanier, *Phys. Rev. C* **46**, 1849 (1992).
 [16] J. B. Gupta and J. H. Hamilton, *Phys. Rev. C* **96**, 034321 (2017).
 [17] M. Sakai, *Nucl. Phys. A* **104**, 301 (1967).
 [18] H. G. Börner, P. Mutti, M. Jentschel, N. V. Zamfir, R. F. Casten, E. A. McCutchan, and R. Krücken, *Phys. Rev. C* **73**, 034314 (2006).
 [19] J. B. Gupta, K. Kumar, and J. H. Hamilton, *Int. J. Mod. Phys. E* **19**, 1491 (2010).
 [20] A. Saha *et al.*, *Nucl. Phys. A* **976**, 1 (2018).
 [21] F. Iachello and N. V. Zamfir, *Phys. Rev. Lett.* **92**, 212501 (2004).
 [22] J. Wiederhold *et al.*, *Phys. Rev. C* **94**, 044302 (2016).
 [23] S. S. Alam *et al.*, *Nucl. Instrum. Methods Phys. Res. A* **874**, 103 (2017).
 [24] J. M. Régis *et al.*, *Nucl. Instrum. Methods Phys. Res. A* **823**, 72 (2016).
 [25] S. S. Alam, T. Bhattacharjee, D. Banerjee, A. Saha, S. Das, M. S. Sarkar, and S. Sarkar, *Phys. Rev. C* **99**, 014306 (2019).
 [26] J.-M. Régis, A. Esmaylzadeh, J. Jolie, V. Karayonchev, L. Knafla, U. Köster, Y. H. Kim, and E. Strub, *Nucl. Instrum. Methods Phys. Res., Sect. A* **955**, 163258 (2020).
 [27] A. Esmaylzadeh *et al.*, *Phys. Rev. C* **98**, 014313 (2018).
 [28] S. K. Basu and A. A. Sonzogni, *Nucl. Data Sheets* **114**, 435 (2013).
 [29] T. Kibédi and R. H. Spear, *At. Data Nucl. Data Tables* **89**, 77 (2005).
 [30] P. Schmelzenbach, K. S. Krane, J. L. Wood, W. D. Kulp, J. Loats, C. J. Staples, and E. B. Norman, *Phys. Rev. C* **98**, 034311 (2018).
 [31] T. Kibédi, T. W. Burrows, M. B. Trzhaskovskaya, P. M. Davidson, C. W. Nestor, Jr., *Nucl. Instrum. Methods Phys. Res., Sect. A* **589**, 202 (2008).
 [32] R. Barlow, Asymmetric Errors, PHYSTAT2003: Statistical Problems in Particle Physics, Astrophysics and Cosmology (Menlo Park, CA, 8-11 September 2003) (SLAC National Accelerator Laboratory), p. 250 (2003).
 [33] A. Possolo, C. Merktas, and O. Bodnar, *Metrologia* **56**, 045009 (2019).
 [34] <https://www.nndc.bnl.gov/ensdf>.